Photoionization of the iodine 3d, 4s, and 4p orbitals in methyl iodide

Ruaridh Forbes, Alberto De Fanis, Cédric Bomme, Daniel Rolles, Stephen T. Pratt, Ivan Powis, Nicholas A. Besley, Marc Simon, Saikat Nandi, Aleksandar R. Milosavljević, Christophe Nicolas, John D. Bozek, Jonathan G. Underwood, and David M. P. Holland

Citation: J. Chem. Phys. **149**, 144302 (2018); doi: 10.1063/1.5035496

View online: https://doi.org/10.1063/1.5035496

View Table of Contents: http://aip.scitation.org/toc/jcp/149/14

Published by the American Institute of Physics

Photoionization of the iodine 3d, 4s, and 4p orbitals in methyl iodide

Ruaridh Forbes,[1,2] Alberto De Fanis,[3] Cédric Bomme,[4] Daniel Rolles,[5] Stephen T. Pratt,[6] Ivan Powis,[7] Nicholas A. Besley,[7] Marc Simon,[8] Saikat Nandi,[9] Aleksandar R. Milosavljević,[9] Christophe Nicolas,[9] John D. Bozek,[9] Jonathan G. Underwood,[1] and David M. P. Holland[10,a)]

[1]*Department of Physics and Astronomy, University College London, Gower Street, London WC1E 6BT, United Kingdom*
[2]*Department of Physics, University of Ottawa, 150 Louis Pasteur, Ottawa, Ontario K1N 6N5, Canada*
[3]*European XFEL GmbH, Holzkoppel 4, 22869 Schenefeld, Germany*
[4]*Deutsches Elektronen-Synchrotron (DESY), 22607 Hamburg, Germany*
[5]*J. R. Macdonald Laboratory, Department of Physics, Kansas State University, Manhattan, Kansas 66506, USA*
[6]*Chemical Sciences and Engineering Division, Argonne National Laboratory, Argonne, Illinois 60439, USA*
[7]*School of Chemistry, University of Nottingham, Nottingham NG7 2RD, United Kingdom*
[8]*Sorbonne Université, UPMC Univ Paris 06, CNRS, UMR 7614, Laboratoire de Chimie Physique-Matière et Rayonnement, F-75005 Paris, France*
[9]*Synchrotron SOLEIL, L'Orme des Merisiers, Saint-Aubin, BP 48, 91192 Gif-sur-Yvette, France*
[10]*Daresbury Laboratory, Daresbury, Warrington, Cheshire WA4 4AD, United Kingdom*

(Received 16 April 2018; accepted 14 September 2018; published online 8 October 2018)

Ionization of the I 3d, 4s, and 4p orbitals in methyl iodide (CH_3I) has been studied by using synchrotron radiation to measure the total ion yield and by recording photoelectron spectra with linearly polarized radiation in two polarization orientations. The complete photoelectron spectrum of CH_3I has been recorded at several photon energies, and bands due to the C 1s, I 3d, 4s, 4p, and 4d atomic-like orbitals, as well as the molecular orbitals, have been observed and assigned. In the vicinity of the I $3d_{5/2}$ and $3d_{3/2}$ ionization thresholds at 626.8 and 638.3 eV, respectively, the ion yield displays weak structure in the pre-edge region due to transitions into valence or Rydberg states, and, at higher energies, a shoulder and a broad maximum attributed to the I $3d_{5/2} \rightarrow \varepsilon$f and the I $3d_{3/2} \rightarrow \varepsilon$f shape resonances, respectively. The absorption spectrum calculated using time-dependent density functional theory, within the Tamm-Dancoff approximation, has allowed assignments to be proposed for the valence and Rydberg states. The Stieltjes imaging technique has been used to simulate the absorption spectrum above the ionization threshold and indicates that transitions into the f(l = 3) continuum channel dominate. This conclusion has been corroborated by a Continuum Multiple Scattering–Xα (CMS–Xα) calculation. The asymmetric broadening of the photoelectron bands associated with the I 3d orbital, due to post collision interaction, is taken into account in our experimental analysis. Experimentally derived photoelectron anisotropy parameters for the I 3d orbital are in good agreement with the theoretical predictions obtained with the CMS–Xα approach. The I 3d shake-up/shake-off photoelectron spectrum has been recorded, and assignments have been proposed for several of the satellites. The $M_4N_{45}N_{45}$ and $M_5N_{45}N_{45}$ Auger electron yields have been measured, and that for the $M_5N_{45}N_{45}$ decay exhibits a maximum due to interchannel coupling between the $3d_{5/2}$ and $3d_{3/2}$ continua. The photoelectron band associated with the I 4p orbital has an unusual appearance. Based upon previous theoretical work for the analogous Xe 4p orbital, it appears that the initial I $4p^{-1}$ hole state decays rapidly through Coster-Kronig and super-Coster-Kronig transitions. This leads to a redistribution of the spectral intensity associated with the I 4p orbital and results in a photoelectron spectrum containing a single structured band together with an extended continuum. Another continuum is observed on the high binding energy side of the peak due to the 4s orbital, and we assign this to super-Coster-Kronig transitions into the $4p^{-1}4d^{-1}$ continuum. *Published by AIP Publishing.* https://doi.org/10.1063/1.5035496

I. INTRODUCTION

Inner-shell photoabsorption and photoionization studies of a molecule containing an atom of high atomic number allow the effect of the molecular environment on the spectroscopic properties and photoionization dynamics of the heavy atom to be investigated. In the present work, the photoion yields and photoelectron spectra associated with the 3d, 4s, and 4p levels of iodine, within methyl iodide (CH_3I), are compared to the corresponding data for xenon. Iodine lies adjacent to xenon in the periodic table, and, for the valence shell, CH_3I is isovalent with Xe. This comparison indicates that many of the photoionization phenomena that have been

a)Electronic mail: david.holland@stfc.ac.uk

studied extensively in connection with the Xe 3d, 4s, and 4p levels also occur for the I 3d, 4s, and 4p atomic-like orbitals in methyl iodide.

The Xe 3d photoionization and photoelectron spectra have long been of considerable experimental and theoretical interest because the energy dependent variations observed in the photoionization partial cross sections and photoelectron angular distributions are a manifestation of strong electron correlation effects.[1–3] Early photoabsorption studies,[4,5] performed with laboratory continuum sources, showed that the 3d spectrum was dominated by two broad maxima located ~11 eV above the $3d_{5/2}$ and $3d_{3/2}$ ionization thresholds, but that the structure due to Rydberg excitations was weak. The two intense maxima were attributed to the $3d_{5/2,3/2} \rightarrow \varepsilon f$ shape resonances.[1,2] The photoelectron spectra,[6,7] measured with monochromatic Al Kα radiation, exhibited a doublet due to the spin-orbit split 3d main-lines, together with some weak peaks ascribed to shake-up satellites.

Later experiments employing synchrotron radiation allowed improved spectra to be recorded and for the ionization process to be studied in greater detail. Specifically, photoabsorption[8,9] and total ion yield[10–12] measurements revealed additional structure and facilitated assignments of the excited states. Of particular interest was an investigation of the photoionization partial cross sections and photoelectron angular distributions for the two spin-orbit ($3d_{5/2}$, $3d_{3/2}$) components.[13] Both of the partial cross sections exhibited a peak due to the $3d \rightarrow \varepsilon f$ shape resonance, but that for the $3d_{5/2}$ channel contained an additional broad maximum that was not predicted in early calculations.[13–16] However, more sophisticated theoretical approaches,[1–3] taking into account many-electron correlations, relativistic effects, and relaxation of the ionic core, revealed that the additional peak is due to interchannel coupling between the $3d_{5/2}$ and $3d_{3/2}$ continua. These theoretical investigations demonstrate that Xe 3d ionization, due to the influence of strong electron correlation effects, provides an ideal means of studying the redistribution of continuum intensity.

Our experimental and theoretical investigations focus on the photoionization of methyl iodide in the photon energy range encompassing the I $3d_{5/2,3/2}$ ionization thresholds and the I $3d_{5/2,3/2} \rightarrow \varepsilon f$ shape resonances. It is of interest to ascertain whether the atomic ionization processes described above for the Xe 3d subshell are observed for the I 3d subshell of the iodine atom within CH_3I. We have measured the total ion yield of CH_3I from just below the I $3d_{5/2}$ ionization threshold up to a photon energy of ~690 eV and interpreted the observed structure with the aid of predictions obtained using time-dependent density functional theory (TDDFT) within the Tamm-Dancoff approximation[17] and the Continuum Multiple Scattering–Xα (CMS–Xα) approach.[18,19] The complete photoelectron spectrum has been recorded at several photon energies, and peaks due to direct photoionization or Auger emission are observed and assigned. These spectra include the region containing the features associated with the nominally I $4p_{3/2}{}^{-1}$ and $4p_{1/2}{}^{-1}$ hole states. The I $3d_{5/2}$ and I $3d_{3/2}$ photoelectron angular distributions and the I $3d_{5/2}$:$3d_{3/2}$ intensity branching ratio have been evaluated from spectra recorded with linearly polarized radiation, at two polarization orientations. The experimentally determined angular distributions are compared to the corresponding CMS–Xα predictions. Finally, the I 3d shake-up/shake-off spectrum has been measured and tentative assignments for some of the observed structure have been proposed based upon valence shell excitation and ionization energies.

In addition to being of fundamental scientific interest, the present studies on the I 3d level in CH_3I are highly relevant to recent time-resolved experiments performed with Free-Electron Lasers (FELs).[20–23] A prerequisite to the interpretation of such time-resolved data is a thorough knowledge and understanding of the spectroscopic properties and photoionization dynamics of the ground state molecule. Time-resolved photoelectron studies in which the ionization is produced through the absorption of a UV photon probe the delocalized valence electrons.[24] In contrast, inner- and core-shell orbitals are strongly localized, and their ionization is element specific and chemically selective. Halogen atom containing molecules have proved particularly suitable for pump-probe studies in the soft X-ray range due to the high photoionization partial cross sections associated with the inner-shell levels. Taking the I 3d subshell as an example, the fundamental spectroscopic and dynamical information required to understand the FEL data includes the spin-orbit resolved photoionization partial cross sections and angular distributions, and photoelectron spectra encompassing the main-lines and the shake-up/shake-off satellites.

II. EXPERIMENTAL APPARATUS AND PROCEDURE

The experiments were carried out on the soft X-ray undulator-based PLÉIADES beamline at the SOLEIL synchrotron radiation facility. Detailed descriptions of the beamline and station instrumentation have been reported previously,[25,26] so only a summary is given here.

The permanent magnet, Apple II type, undulator provides linearly polarized synchrotron radiation in the energy range 35–1000 eV, with the degree of polarization being estimated to be >99%. The linear polarization can be rotated through 90°, thereby enabling photoelectron angular distributions to be determined with an electron analyser in a fixed position. Two prefocussing mirrors are used to deliver the radiation into a plane grating, modified-Petersen type,[27] monochromator. The photoion and photoelectron spectra were recorded with a grating having 600 lines/mm. An exit slit width of 10 μm was chosen, resulting in a theoretical optical resolution which varies between ~80 meV at hυ = 630 eV and ~100 meV at hυ = 750 eV, for the photoelectron spectra encompassing only the I 3d peaks. Alternatively, an exit slit width of 70 μm was chosen, resulting in a theoretical optical resolution of ~300 meV, for the complete photoelectron spectra covering the entire energy range (to include all peaks extending from those due to direct ionization of the valence orbitals to those due to the carbon KVV Auger electrons).

Two spectrometers were employed in our experimental studies: (i) a channelplate detector for measuring the total ion yield, and (ii) a VG Scienta R4000 analyser for recording electron spectra.

The ion spectrometer, described in supplementary material, was used to record the total yield between 610 and 690 eV, in 50 meV steps. The energy scale was calibrated by measuring a spectrum of a mixture of CH_3I, O_2, and Xe in the energy range 527–680 eV and making use of the established transition energies of 530.5 and 539.5 eV for the $2p\pi^*$ and $2p\sigma^*$ resonances in O_2[28] and 674.0 eV for the $3d_{5/2} \rightarrow 6p$ Rydberg excitation in Xe.[9]

Electron spectra, for emission either parallel or perpendicular to the polarization vector of the linearly polarized radiation, were recorded with the Scienta analyser. This spectrometer, mounted with the electron detection axis lying perpendicular to the plane of the electron orbit in the storage ring, was operated in the transmission mode of the electron lens. The sample gas was flowed into a differentially pumped cell which contains a series of electrodes to correct for the plasma potentials generated along the path of the synchrotron radiation.[29] Spectra were recorded using analyser pass energies of 5, 10, 20, or 50 eV, and a 0.6 mm curved entrance slit, resulting in theoretical spectrometer resolutions of 10, 20, 40, or 100 meV, respectively.

The translational Doppler broadening, associated with the thermal motion of the room temperature CH_3I sample, also contributes to the observed peak width. The linewidth due to this broadening, ΔE_D, is given by $\Delta E_D(\text{meV}) = 0.7215 (E_{KE} \cdot T/M)^{1/2}$, where E_{KE} is the electron kinetic energy in eV, T is the absolute temperature of the sample gas, and M is the molecular mass expressed in atomic units.[29] For the maximum photon energy, 750 eV, used to ionize the I 3d shell in CH_3I, ΔE_D is ~11.5 meV.

The electron spectrometer employs a camera-based MCP/phosphor screen detector setup and was operated in pulse counting mode. In this mode, each illuminated pixel on the CCD camera has a thresholding applied such that the signal is proportional to a single electron count. This procedure ensures good linearity, thereby allowing the number of counts to be extracted.

For completely linearly polarized radiation, the photoionization differential cross section in the electric dipole approximation, assuming randomly oriented target molecules and electron analysis in a plane perpendicular to the photon propagation direction, can be expressed in the form[30]

$$\frac{d\sigma}{d\Omega} = \frac{\sigma}{4\pi}[1 + \beta P_2(\cos\theta)], \tag{1}$$

where σ is the angle integrated cross section, β is the photoelectron anisotropy parameter which characterises the angular distribution, θ is the photoelectron ejection angle relative to the polarization axis, and P_2 is a second order Legendre polynomial: $P_2(\cos\theta) = (3\cos^2\theta - 1)/2$.

Alternatively, the anisotropy parameter can be expressed in the experimentally convenient form[26]

$$\beta = \frac{2(I_{par} - I_{perp})}{(I_{par} + 2I_{perp})}, \tag{2}$$

where I_{par} and I_{perp} are the normalized electron intensities for parallel ($\theta = 0°$) and perpendicular ($\theta = 90°$) polarization orientations relative to the electron detection axis, respectively. All the spectra were normalized to the sample pressure, the accumulation time, and the photon flux (which was measured with a photodiode located at the end of the beamline) prior to processing.

The electron kinetic energy scale was calibrated using the established binding energies of the Xe $3d_{5/2,3/2}$ lines[31] and the known energies of various Auger lines in Xe.[32] The transmission efficiency of the electron analyser was determined, as described by Jauhiainen *et al.*,[33] and all the plotted spectra have been corrected for this variation.

III. THE EFFECT OF POST COLLISION INTERACTION ON THE I 3d PHOTOELECTRON PEAK SHAPE

In the present experiment, photoelectron spectra of the I $3d_{5/2}$ and I $3d_{3/2}$ levels were recorded in the photon energy range 630–750 eV, resulting in electron kinetic energies of ~5–120 eV. The initially created 3d hole decays through the emission of Auger electrons having kinetic energies in the ~350–570 eV range. When the photon energy lies only slightly above the inner-shell ionization threshold, as in our work, the slowly departing photoelectron may be additionally influenced by the Auger electron. The resulting interaction between the two escaping electrons is termed post collision interaction (PCI).[34,35] Classically, PCI can be described as the change in the mutual shielding of the two departing electrons. Close to threshold, where the kinetic energy of the photoelectron is low, this slowly receding electron shields the doubly charged ion. Energy is exchanged between the two outgoing electrons, with the Auger electron gaining energy and the photoelectron losing a similar amount. PCI results in the photoelectron peak shape exhibiting a characteristic asymmetry toward low kinetic energies.

The adoption of a fitting routine to analyze the experimental photoelectron data, rather than using the integrated signal within a peak, has two advantages: (i) the fitting can allow the widths relating to the experimental and core-hole broadening to be extracted, and (ii) the background intensity can be modelled more accurately and the associated contributions removed from further analysis. The effect of the PCI distortion on the shape of the I 3d photoelectron peaks was taken into account in our analysis by incorporating the approximate line shape described by Armen *et al.*[36] A full description of the fitting routine, and the procedure used to obtain the global error function, is described in the supplementary material. The error bars shown in our figures represent the standard error on the fitting parameters.

IV. THEORETICAL TECHNIQUES

A. Calculation of the absorption spectrum using the TDDFT method

The absorption spectrum of CH_3I was computed using TDDFT within the Tamm-Dancoff approximation.[17] In this approximation, the coupling matrix (usually denoted **B**) of the TDDFT equations is assumed to be zero, and as a consequence only occupied to virtual transitions are included, with the virtual to occupied transitions being neglected. In our calculations on CH_3I, the single excitation space was limited to include just excitations from the five iodine 3d orbitals

to the full virtual orbital subspace.[37] The calculations used the CAM-B3LYP exchange-correlation functional[38] with an augmented quadruple zeta plus polarization basis set.[39] The calculations do not include relativistic effects. We denote the computed spectrum, due to excitation or ionization of an I 3d electron, as I $3d_{5/2}^{-1}$. The I $3d_{3/2}^{-1}$ spectrum is then generated by shifting the computed I $3d_{5/2}^{-1}$ spectrum by +11.48 eV. This energy shift corresponds to the I 3d spin-orbit splitting measured in the present experiment. The ionization threshold relative to the lowest energy transition ($3d \rightarrow \sigma^*$) in the neutral molecule is computed using a ΔSCF approach.[40] Using this approach, the energy difference is determined to be 6.77 eV. Combining this value with the TDDFT calculations gives ionization energies of 627.17 eV for I $3d_{5/2}^{-1}$ and 638.65 eV for I $3d_{3/2}^{-1}$. For comparison, our corresponding experimental results, discussed below, are 626.8 and 638.3 eV. The spectrum above the ionization threshold is simulated using the Stieltjes imaging technique[41] with the discrete transition energies and intensities computed using TDDFT. The spectrum below the ionization threshold is generated by convoluting the calculated intensity at each transition energy with a Gaussian of 0.5 eV (FWHM). The spectrum for the pre-threshold region is combined with that for the post-threshold region to generate the total spectrum.

B. Calculation of the I 3d photoionization partial cross section and the photoelectron anisotropy parameter using the CMS–Xα approach

Photoionization partial cross sections and photoelectron anisotropy parameters were calculated by following the method and details as previously described,[42] and subsequently modified,[43] in our earlier investigations of methyl iodide.

Briefly, electric dipole photoionization matrix elements are calculated using the CMS–Xα method.[42] A model molecular potential having the molecular volume partitioned into overlapping spherical regions centred on each atomic centre, all enclosed within an outer spherical region centred on the I atom, is first constructed. The asymptotic form is adjusted to have the correct long range ion-electron Coulombic interaction. Continuum electron wavefunctions are then generated using multiple scattering equations with a symmetry adapted spherical harmonic angular basis, truncated for these calculations at $l_{max} = 8$ (outer sphere), 7 (I atoms), 6 (C atoms), and 4 (H atoms). Using the orthogonal set of bound orbital functions available from the Xα potential, the one-electron (frozen core) dipole matrix elements for specific ionization channels of interest are then calculated, from which the photoionization partial cross section and the photoelectron anisotropy parameter (σ and β) are obtained.

V. RESULTS AND DISCUSSION

A. Experimental total ion yield and calculated absorption and photoionization spectra

Figure 1 shows the total ion yield spectrum of CH_3I recorded in the vicinity of the I 3d ionization thresholds. The yield, which is generally similar to the electron energy loss spectrum measured by Hitchcock and Brion,[44] exhibits a broad

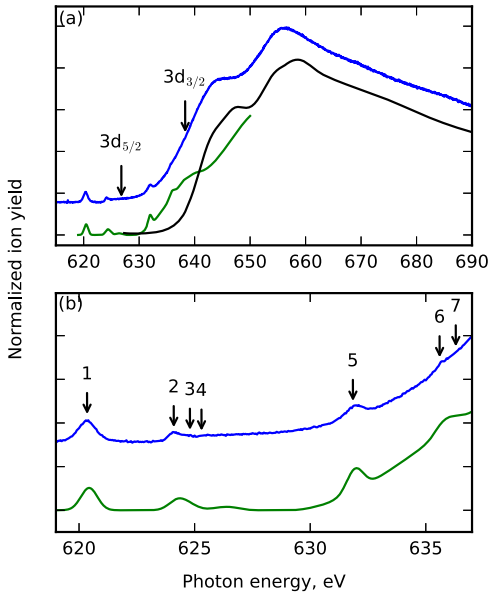

FIG. 1. (a) The experimental total ion yield (blue) of CH_3I recorded in the photon energy range 610–690 eV using parallel linearly polarized radiation. The theoretical absorption spectrum (green) calculated using the TDDFT method and the photoionization cross section (black) calculated using the CMS–Xα approach are also shown. The I $3d_{5/2}$ and I $3d_{3/2}$ ionization thresholds at 626.8 and 638.3 eV, respectively, are marked. (b) Expanded sections of the spectra showing the threshold region in greater detail. The arrows denote the positions of resonances. The measured and predicted excitation energies of these resonances are given in Table I. In (a) and (b), the lowest tick on the y axis corresponds to the true zero of the experimental yield measurement.

maximum at ~656 eV and a shoulder at ~644 eV. The separation (~12 eV) between these features is comparable to the I 3d spin-orbit splitting (11.48 eV) determined in the present study. The shoulder and maximum can be attributed to the $3d_{5/2} \rightarrow \varepsilon f$ and $3d_{3/2} \rightarrow \varepsilon f$ shape resonances, respectively, based on the corresponding observed[4,5,10–13,44] and predicted[1,2] processes in Xe.

The experimental ion yield (Fig. 1) exhibits several features in the pre-edge region which are not evident in the earlier electron energy loss spectrum of CH_3I.[44] Somewhat similar structure has been observed in the Xe 3d absorption[5,9] and ionization[11,12] spectra, and attributed to excitation of the $3d_{5/2,3/2}$ electrons into p-type Rydberg orbitals. Figure 2 shows the peaks appearing in our ion yield below the ionization thresholds in greater detail. The TDDFT results (Fig. 2) have been plotted after convoluting the spectral intensity at a particular excitation energy with a Gaussian of 0.1 eV (FWHM), allowing the individual contributions to be discernible, and after convoluting with a Gaussian of 0.5 eV (FWHM), to provide a better match with the experimental spectrum. The convoluted data illustrate that a single broadening is not optimal for all of the bands appearing in the spectrum. The observed variation in the experimental peak width may be a consequence of the different lifetimes of the excited states. Orbital plots for some of the low lying excited states are also shown in Fig. 2. Overall, the computed spectrum is in good agreement with the experimental measurements, particularly in the pre-edge region. It should be noted that the experimental total ion yield shown in Fig. 1 includes contributions from valence shell ionization in addition to the contribution from the I 3d shell, whereas both

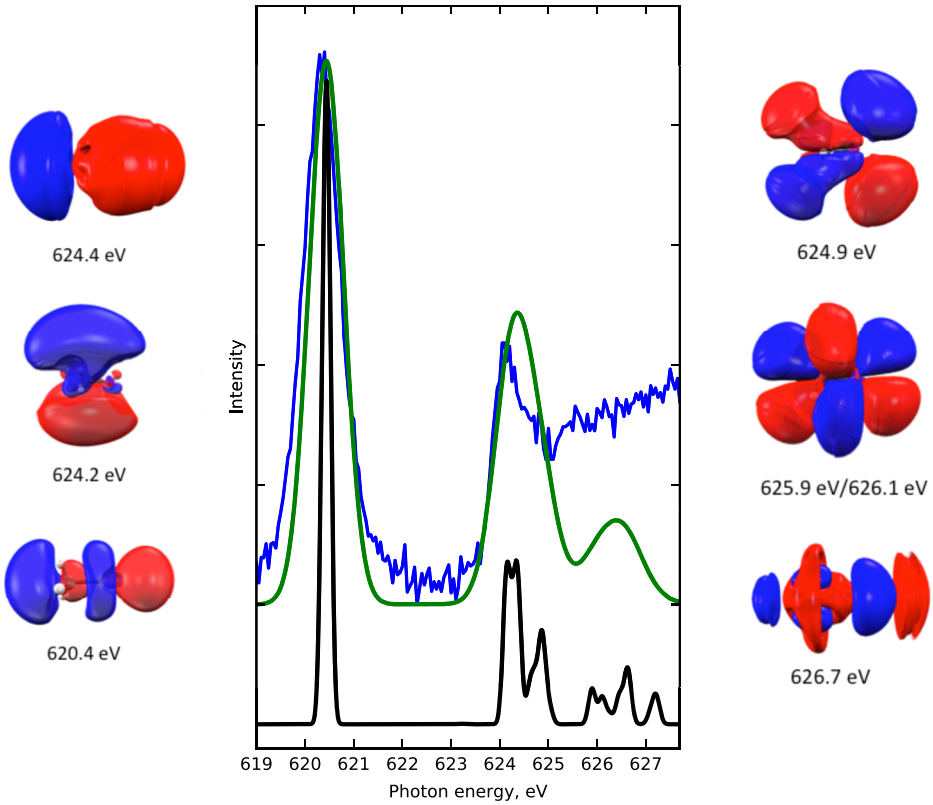

FIG. 2. The experimental total ion yield (blue) of CH_3I in the I $3d_{5/2}$ threshold region. The theoretical (TDDFT) absorption spectrum is shown after convolution of the calculated spectral intensity at a particular excitation energy with a Gaussian of 0.1 eV (FWHM) (black) to allow the individual contributions to be discernible, and after convolution with a Gaussian of 0.5 eV (FWHM) (green) to provide a better match with the experimental spectrum. Plots of the valence and Rydberg orbitals, together with the corresponding calculated transition energies associated with excitation from the I $3d_{5/2}$ orbital, are shown. In the orbital plots, the carbon-iodine bond lies horizontally with the methyl group on the left; iso-surface values of 0.02 a.u. for the σ^* orbital and 0.03 a.u. for the Rydberg orbitals are used.

theoretical results are associated with the I 3d shell only. This accounts for the vertical shift evident between the experimental and calculated spectra.

Our calculations neglect an explicit description of relativistic effects and there will also be some error associated with the use of the CAM-B3LYP exchange-correlation functional for the transitions from the inner-shell orbitals.[45] Therefore, it is possible that the close agreement between the calculated and experimental excitation energies arises in part from a cancellation of errors. The energies of the excitations from the different d orbitals are not degenerate, and the energies shown in Fig. 2 and listed in Table I correspond to the energy of the peak of the bands resulting from the convolution with the Gaussian functions. Oscillator strengths are also given in Table I.

The first band, labeled as peak 1 in Fig. 1(b), is computed to lie at 620.4 eV compared to the experimental value of 620.35 eV. This band arises from transitions from the $3d_{5/2}$ orbital into the lowest unoccupied $\sigma^*(a_1)$ molecular orbital, which has antibonding character along the carbon-iodine (C–I) axis. In a similar manner, peak 5, observed at 631.95 eV, is attributed to the $3d_{3/2} \rightarrow \sigma^*(a_1)$ transition. As the I 3d spin-orbit splitting is 11.48 eV, bands due to excitations involving the $3d_{3/2}$ orbital are embedded in the $3d_{5/2}^{-1}$ continuum.

The next distinct band, due to excitation from the I $3d_{5/2}$ orbital, in the experimental spectrum is probably an unresolved doublet with maxima at ~624.1 eV (peak 2) and 624.8 eV (peak 3). Our theoretical predictions (Table I) indicate that the maximum at 624.1 eV arises from transitions into two p-type orbitals lying perpendicular (pe) and parallel (pa_1) to the C–I bond. The calculated excitation energies for these two Rydberg transitions are 624.2 and 624.4 eV, respectively. The higher energy side of this doublet is predicted to have contributions from transitions into orbitals that have Rydberg d character. Finally, there is tentative evidence in the experimental spectrum of a peak at 625.4 eV (peak 4). The nature of the orbitals for the higher energy bands becomes increasingly complex to

TABLE I. Excitation energies and proposed assignments for structure in the total ion yield of CH_3I due to valence and Rydberg states belonging to series (i) converging onto the $3d_{5/2}$ ionization threshold and (ii) converging onto the $3d_{3/2}$ ionization threshold.

Spectral feature	Excitation energy (eV) Experimental	Theoretical[a]	Assignment
(i)			
1	620.35	620.4(0.0025)	$3d_{5/2} \rightarrow \sigma^*(a_1)$
2	624.1	624.2(0.0006)/624.4(0.0005)	$3d_{5/2} \rightarrow 6pe/6pa_1$
3	624.8	624.9(0.0001)	$3d_{5/2} \rightarrow d$
4	625.4		$3d_{5/2} \rightarrow$ unassigned
$3d_{5/2}$ IE	626.8[b]	626.17	$3d_{5/2} \rightarrow \infty$
	644.4		$3d_{5/2} \rightarrow \varepsilon f$
(ii)			
5	631.95	631.9(0.0025)	$3d_{3/2} \rightarrow \sigma^*(a_1)$
6	635.7	635.7(0.0006)/635.9(0.0005)	$3d_{3/2} \rightarrow 6pe/6pa_1$
7	636.4	636.4(0.0001)	$3d_{3/2} \rightarrow d$
$3d_{3/2}$ IE	638.3[b]	638.67	$3d_{3/2} \rightarrow \infty$
	656.0		$3d_{3/2} \rightarrow \varepsilon f$

[a]Oscillator strengths are given in the parentheses and represent the sum of the contributions to the spectral band from the different 3d orbitals.
[b]Ionization energies (IEs) measured in the present experiment.

assign in the calculated spectrum, so an accurate description of the predicted and observed structure is no longer feasible.

The assignments for peaks 6 and 7, due to excitations originating from the $3d_{3/2}$ orbital, are analogous to those given for peaks 2 and 3.

The TDDFT calculations show that the continuum intensity arises from transitions to f orbitals. Figure 3(a) illustrates two typical orbitals corresponding to the discrete states which contribute significant oscillator strength to the continuum. These orbitals have features which are characteristic of an f orbital localized around the iodine atom. The basis set used in the calculations contains basis functions with angular momenta up to and including l = 5(h) functions. Removing the higher angular momentum basis functions from the basis set has the effect of removing transitions to these states from the calculations. This allows the nature of the states contributing to the continuum to be examined. Figure 3(b) shows the computed continuum region when the l = 4(g) and l = 5(h) basis functions have been removed, and also when the l = 3(f), 4, and 5 basis functions have been removed. When the g and h functions are removed, there is only a minor loss in intensity, suggesting that these states do not make a significant contribution to the continuum. In contrast, the intensity in the continuum is reduced almost to zero when the f functions are removed, thereby showing that transitions to these states make the dominant contribution to the continuum. Note that the apparent higher intensity, around 630 eV, associated with the curve having the l = 3, 4, and 5 basis functions removed compared to that having only the l = 4 and 5 basis functions removed, and that having all the functions present, is an artefact of the spline fitting used in the Stieltjes image fitting procedure.

The I 3d photoionization cross section of CH_3I, calculated using the CMS–Xα approach, is shown in Fig. 1(a). The split $3d_{5/2,3/2}$ threshold is simulated by repeating the calculation (which neglects spin-orbit interaction) assuming the two experimental ionization energies and then summing these cross sections with an appropriate statistical weighting. It is evident that, apart from a small energy offset of a few eV, the CMS-Xα calculation captures the f-wave shape resonance in the cross section(s) very effectively. In comparison with the TDDFT results, it is seen that while the latter captures the near-edge structure well, the TDDFT calculations are unable to include enough of the high energy excitations to provide a reliable estimate of the intensity in the continuum region, which starts to fall away. In contrast, the continuum multiple scattering CMS-Xα approach provides a good account of the shape of the photoionization cross section above threshold but omits the resonances around threshold.

These CMS-Xα cross section results are examined more closely in Figs. 4(a) and 4(b) which display the cross section decomposition into partial l-wave contributions. It is evident that the l = 3(f) wave makes the dominant contribution to the

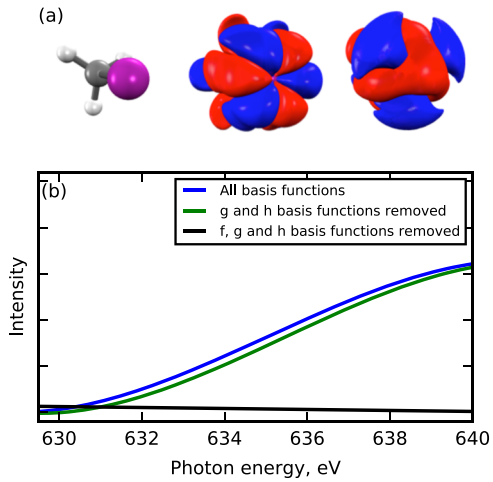

FIG. 3. (a) Two orbitals, typical of those involved in the transitions which give rise to the oscillator strength in the continuum. The TDDFT calculations indicate that these orbitals have features characteristic of an f orbital localized around the iodine atom (an iso-surface value of 0.03 a.u. is used). (b) Theoretical absorption spectra, calculated using TDDFT, as a function of the employed basis set.

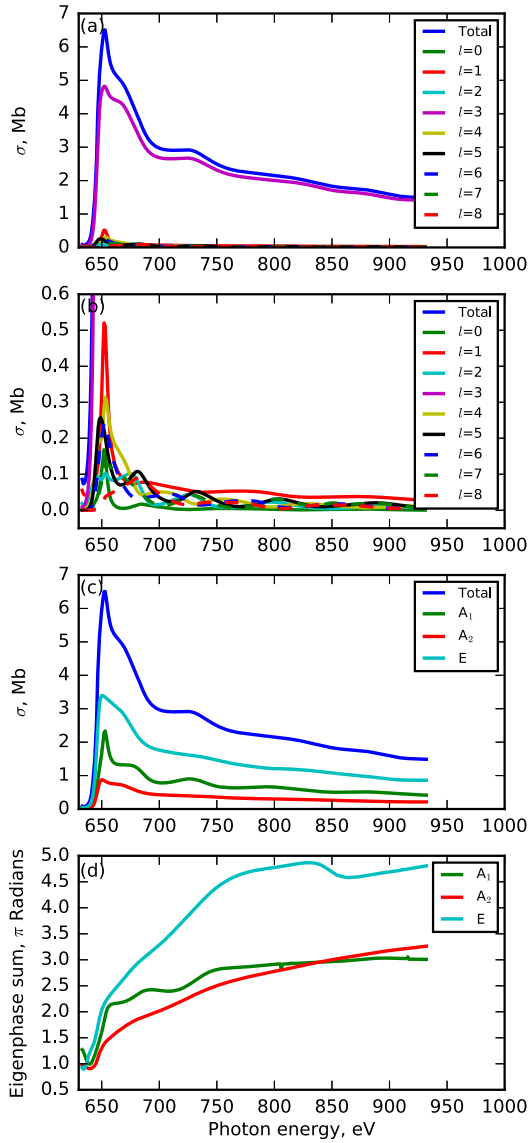

FIG. 4. (a) Photoionization cross section of the I 3d level in CH_3I, calculated using the CMS–Xα approach, decomposed into partial l-wave contributions, and expanded around the I atom. (b) Photoionization cross sections expanded to highlight the weaker l-wave contributions. (c) Photoionization cross sections decomposed into contributions made by symmetry adapted combinations of the angular basis functions. (d) The symmetry adapted eigenphase sums.

I 3d photoionization cross section, as expected for an atomic-like process, and in accord with the TDDFT results. In Fig. 4(c) we present an alternative decomposition of the cross section into symmetry adapted combinations of the continuum angular basis functions. In this view, it is seen that the a_2, a_1, and e symmetry continua maintain an approximate 1:2:4 weighting across the whole energy range. This reflects the number of f-wave *m* substates of each symmetry type, suggesting that these substates each may make similar overall contributions to the ionization.

The theoretical spectrum displays a peak at a kinetic energy of ~20.5 eV above the ionization threshold, readily attributable to the expected 3d → εf shape resonance. The eigenphase sums [Fig. 4(d)] identify, for both the a_1 and e continua, a sharp phase rise of ~π radians at this energy, providing a signature indication of the presence of shape resonances in both of these partial channels. It should be noted, however, that apart from the region around 650 eV where the $l = 1$ component is the second most dominant partial wave, $l \geq 3$ partial waves make significant contributions, thereby underlining some molecular character existing in the ionization process.

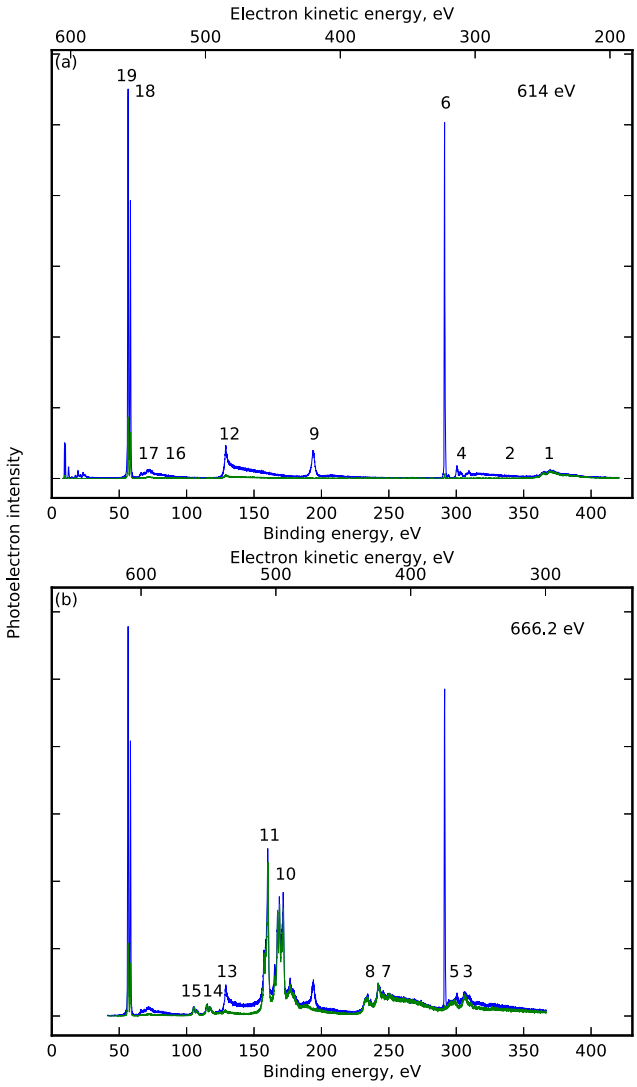

FIG. 5. (a) The electron spectrum of CH_3I recorded at a photon energy of 614.0 eV using parallel (blue) and perpendicular (green) linearly polarized radiation. Most of the structure is due to direct photoionization. (b) The electron spectrum of CH_3I recorded at a photon energy of 666.2 eV using parallel (blue) and perpendicular (green) linearly polarized radiation. Most of the structure in the spectrum recorded with perpendicular linearly polarized radiation is associated with the $M_{45}N_{45}O_{23}$, $M_{45}N_{45}V$, $M_{45}N_{45}N_{45}$, $M_{45}N_{23}N_{45}$, and $M_{45}N_1N_{45}$ Auger transitions. The numbered peaks in (a) and (b) are identified in Table II.

B. Photoelectron spectra

1. Overview of the complete spectrum

Figure 5(a) shows the photoelectron spectrum of CH_3I, measured at a photon energy of 614 eV, for parallel and perpendicular linearly polarized radiation. This energy lies below the I 3d ionization thresholds and the spectrum is dominated by bands due to ionization of the C 1s and I 4d levels. The photoelectron bands associated with the valence shell are relatively weak. Bands due to direct photoionization can be assigned using the previously reported binding energies of the C 1s(291.3 eV[44]), I 4s(195.4 eV[6,31]), I 4p(~129 eV[46]), I 4d(58.3 eV - $4d_{3/2}$, 56.7 eV - $4d_{5/2}$[47]), and valence[43,48] orbitals. Some weak structure associated with the I 4d and C 1s shake-up/shake-off transitions is also discernible.

A section of the spectrum recorded at a photon energy of 666.2 eV, which lies above the I 3d ionization thresholds, is plotted in Fig. 5(b). The additional structure occurring in this spectrum arises from various Auger decay channels associated with the M_4 and M_5 subshells. The photoelectron peaks due to the I $3d_{5/2,3/2}$ levels are not included in Fig. 5(b) and will be discussed in Secs. V B 3 and V B 4. Table II provides a summary of the photoelectron and Auger electron bands appearing in the experimental spectrum. Peaks due to direct ionization or shake-up/shake-off transitions are referenced with respect to their binding energy, whereas those due to Auger transitions

TABLE II. Energies and assignments of the bands observed in the electron spectra of CH_3I shown in Fig. 5.

Spectral feature	Electron kinetic energy (eV)	Binding energy (eV)	Assignment
1	~220–265		C KVV
2		316–366	C 1s shake-off
3	~355–363		$M_5N_1N_{45}$
4		294–316	C 1s shake-up
5	~365–373		$M_4N_1N_{45}$
6		291.3	C 1s
7	~413–426		$M_5N_{23}N_{45}$
8	~426–437		$M_4N_{23}N_{45}$
9		193.8	I 4s
10	~488–500		$M_5N_{45}N_{45}$
11	~500–512		$M_4N_{45}N_{45}$
12		129.0	I 4p
13	~530–545		$M_{45}N_{45}V$
14	~546–554		$M_5N_{45}O_{23}$
15	~556–564		$M_4N_{45}O_{23}$
16		76–102	I 4d shake-off
17		62–76	I 4d shake-up
18		58.3	I $4d_{3/2}$
19		56.7	I $4d_{5/2}$

are referenced with respect to their electron kinetic energy. The electron peaks arising from Auger decay of the M_4 and M_5 subshells, and their associated angular distributions, are discussed in detail by Forbes *et al.*[49]

2. Photoelectron bands associated with the I 4s and I 4p orbitals

Figure 6(a) shows the region of the photoelectron spectrum encompassing structure associated with the I 4s and I 4p orbitals in greater detail. Our spectrum is broadly in accord with those measured by Gelius[6] and by Svensson *et al.*[31] using Al Kα radiation, but is of improved quality and covers a wider binding energy range. The anomalous appearance of the photoelectron bands is similar to that observed in Xe.[6,7,31]

The earliest indication of the unusual behavior of the Xe 4p orbital was found in the absorption spectrum[50,51] where lines were observed converging onto what was considered to be the $4p^5\ ^2P_{3/2}$ ionization threshold, whereas none were evident converging onto the $4p^5\ ^2P_{1/2}$ threshold. Confirmation of this anomaly was provided by the photoelectron spectrum[6,7,31] which, instead of exhibiting a well-resolved spin-orbit doublet associated with the 4p orbital, showed a single structured peak in the vicinity of the expected $4p^5\ ^2P_{3/2}$ ionization limit, together with a continuous intensity distribution which extended up to a second peak, which was associated with the $4s\ ^1S_0$ limit.

This anomalous intensity distribution is a consequence of strong electron correlation, resulting in a breakdown of the single particle model of ionization.[52] Under such circumstances, the two-step model of Auger decay,[53] where photoionization forms a well-defined core hole and the subsequent emission of the Auger electron is considered to be an independent process, becomes invalid. Instead, the inner-shell hole state transforms rapidly, through Coster-Kronig and super-Coster-Kronig processes, into excited states having configurations with two excited electrons. Coster-Kronig[54] and super-Coster-Kronig[55] transitions correspond to Auger decays in which one, or both, respectively, of the holes in the final ionic state belongs to the same principal shell as the initial vacancy. Such processes have very high transition rates.

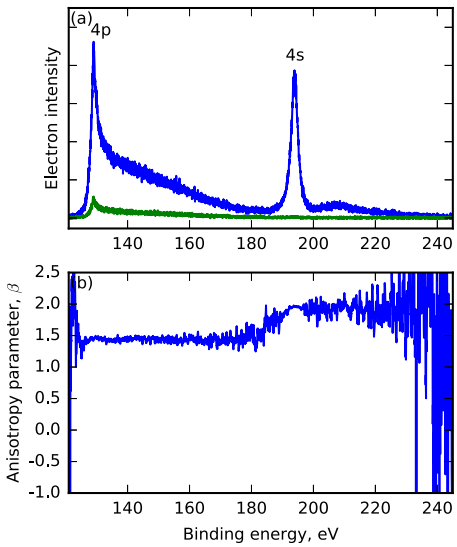

FIG. 6. (a) Photoelectron spectrum of CH_3I, recorded at a photon energy of 614.0 eV, using parallel (blue) and perpendicular (green) linearly polarized radiation, in the binding energy range encompassing structure due to the I 4s and I 4p orbitals. (b) The corresponding photoelectron anisotropy parameter. A 10-point moving average has been applied to the anisotropy parameter spectrum to improve the signal-to-noise ratio.

To provide the framework required to interpret our photoelectron spectra of the I 4s and 4p levels in CH_3I, we give a brief summary of the theoretical studies performed by Wendin and Ohno[56,57] on the corresponding Xe 4s and 4p levels. For the initially formed $4p^{-1}$ state, the following decay mechanisms were considered[56,57] (using the nomenclature adopted in previous discussions[56–59]): $4p^{-1} \rightarrow 4d^{-1}5p^{-1}$ + kl electron, Coster-Kronig transition; $4p^{-1} \rightarrow 4d^{-1}5s^{-1}$ + kl electron, Coster-Kronig transition; $4p^{-1} \rightarrow 4d^{-2}$ + kl electron, super-Coster-Kronig transition; and $4p^{-1} \rightarrow 4d^{-2}$ + 4f electron, giant-Coster-Kronig transition (where k denotes a discrete or continuum orbital). The calculations showed that the dominant decay process yields $4d^{-2}$kl electron configurations and that the peak observed in the vicinity of the expected $4p^5\ ^2P_{3/2}$ threshold should be attributed to a group of satellites with electron configurations $4d^{-2}$kf, of which $4d^{-2}4f\ ^2P_{3/2}$ is the strongest component. This peak was predicted to have only 38% of the spectral intensity associated with the unperturbed 4p photoionization, and its binding energy is shifted with respect to that calculated for the unperturbed state. The other decay mechanisms listed above are responsible for the continuum observed between the peaks due to the $4d^{-2}4f\ ^2P_{3/2}$ and the $4s\ ^1S_0$ states.

For the initially formed $4s^{-1}$ state, the decay mechanisms considered[56,57] were $4s^{-1} \rightarrow 4p^{-1}4d^{-1}$ + kl electron, $4s^{-1} \rightarrow 4p^{-1}5s^{-1}$ + kl electron, and $4s^{-1} \rightarrow 4p^{-1}5p^{-1}$ + kl electron.[56–59] Although these interactions lead to a shift in the binding energy of the peak associated with the 4s orbital with respect to the unperturbed value, most of the spectral intensity (~80%) remains in a single peak. Thus, this peak may be characterized as being due to a reasonably well defined hole of mainly 4s character. The remaining part of the 4s intensity was predicted to appear in the super-Coster-Kronig $4p^{-1}4d^{-1}$ continuum.[56,57] This prediction could not be verified because the experimental spectrum did not extend to sufficiently high binding energies.

The photoelectron band shapes associated with the I 4p and I 4s orbitals in CH_3I are similar to those discussed above in relation to the corresponding orbitals in Xe, and thus similar configuration interactions and decay mechanisms appear to apply. We obtain binding energies of 129.0 and 193.8 eV for the maxima of the peaks due to the 4p and 4s orbitals, respectively. The I 4p peak shows some hints of structure on the high binding energy side. The analogous structure observed on the Xe 4p peak was associated with multiplets within the $(4d^{-2}4f)_{3/2}$ configuration.[56] A fitting of the peak due to the I 4s orbital, with a Voigt profile, results in a Lorentzian of 2.43 eV (FWHM), representing the hole state level width, and a Gaussian of 0.56 eV (FWHM), representing the experimental resolution. Thus, the level width of the peak due to the I 4s orbital is similar to that (2.7 eV[31]) for the corresponding Xe 4s peak. Our spectrum shows a continuum in the binding

energy range ~200–250 eV. We attribute this continuum to the decay of the I 4s hole state into the $4p^{-1}4d^{-1}$ continuum, via super-Coster-Kronig transitions, as predicted for the 4s hole state in Xe.[56,57]

Figure 6(b) shows the β parameter, evaluated using Eq. (2), as a function of the binding energy in the region of the I 4s and 4p photoelectron peaks. It is evident that the value of the β parameter associated with the continuum occurring on the high binding energy side of the principal peak due to the 4p orbital is similar to that in the peak. The same behavior is observed for the β parameter corresponding to the 4s peak and that of the continuum appearing at higher binding energies. At a photon energy of 614 eV, we obtain a β value of 2.0 for the I 4s peak (by integrating between binding energies of ~188–200 eV). We obtain β values of 1.4, 1.1, 1.3, and 1.0 at photon energies of 614, 620.1, 656, and 666.2 eV, respectively, when we evaluate the intensity around a small energy range containing the I 4p line. These values are similar to those measured by Becker *et al.*[60] for the 4s and 4p orbitals in Xe in the vicinity of the Xe 3d threshold. It was suggested[60] that the variations in the Xe 4s β parameter, close to the 3d edge, might be due to interchannel coupling between the 4s and 3d subshells. A similar type of coupling might be the cause of the variations we observe in the β values for the I 4p peak in the vicinity of the I 3d threshold.

3. Photoelectron bands associated with the I $3d_{5/2,3/2}$ orbitals

Figure 7 shows the photoelectron spectrum of CH_3I, recorded at a photon energy of 665.6 eV, in the binding energy region encompassing the two peaks associated with the I $3d_{5/2}$ and $3d_{3/2}$ electrons. The bands exhibit a characteristic tailing toward higher binding energy due to PCI. For both of the spin-orbit split states, the peak binding energy, intensity, β parameter, and level width of the hole state were extracted by performing a weighted least-squares fit to the spectra (see the supplementary material).

The binding energies of the I $3d_{5/2,3/2}$ levels in CH_3I have not been reported previously. We recorded the photoelectron spectrum of a mixture of CH_3I and Xe, in the binding energy range containing the I 3d and Xe 3d peaks. There are several earlier measurements of the Xe $3d_{5/2,3/2}$ binding energies.[6,31,61] Those of Svensson *et al.*[31] were used to calibrate our binding energy scale and resulted in energies of 626.8 and 638.3 eV, with an estimated uncertainty of ±0.4 eV, for the I $3d_{5/2}$ and I $3d_{3/2}$ ionization thresholds, respectively. This uncertainty is related to the spread in the previously reported Xe binding energies[6,31,61] available for use as calibrations rather than to any limitation in our experimental instrumentation. The I 3d photoelectron spectra also allow the spin-orbit splitting to be determined. We obtain a value of 11.48 ± 0.01 eV from an analysis of our spectra recorded at thirteen photon energies.

Level widths between 440–520 meV and 450–500 meV were obtained from our fitting procedure for the I $3d_{5/2}$ and $3d_{3/2}$ hole states in CH_3I, respectively. These values are in reasonable accord with those of $\Gamma_{5/2}$ = 510 ± 30 meV and $\Gamma_{3/2}$ = 490 ± 30 meV for the corresponding 3d hole states in Xe.[62]

Figure 8 shows the experimentally derived I $3d_{5/2}$ and I $3d_{3/2}$ photoelectron anisotropy parameters. The predictions of the (non-relativistic) CMS–Xα calculations, which have been plotted using the experimental ionization energies of 626.8 and 638.3 eV, are in good agreement with the measured values. The β parameter is predicted to be negative near threshold and then to rise rapidly as the photon energy increases to reach a maximum close to unity ~15 eV above threshold. The photon energies at which these maxima occur, ~640 and 655 eV for the $3d_{5/2}$ and $3d_{3/2}$ orbitals, respectively, approximately coincide with those for the predicted $3d_{5/2} \rightarrow \varepsilon f$ and $3d_{3/2} \rightarrow \varepsilon f$ shape resonances. At higher energies, the experimental and calculated β parameters gradually decrease. Our theoretical work indicates that the dip around hν = 700 eV may be associated with a (weak) extended X-ray absorption fine structure type oscillation occurring in the a_1 symmetry continuum function [Fig. 4(c)]. The localization of the initial 3d

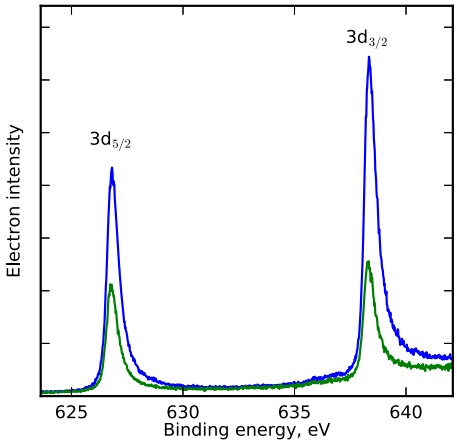

FIG. 7. Photoelectron spectrum of CH_3I, recorded at a photon energy of 665.6 eV, using parallel (blue) and perpendicular (green) linearly polarized radiation. The two bands are due to ionization of the I $3d_{5/2}$ and I $3d_{3/2}$ levels. The asymmetric band shapes are the result of post collision interaction.

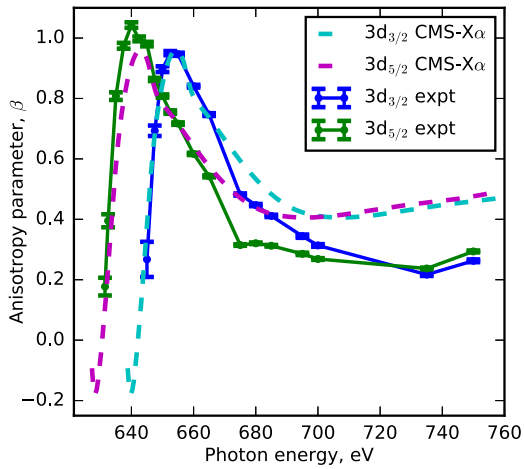

FIG. 8. The experimentally derived photoelectron anisotropy parameters for the I $3d_{5/2}$ (green) and I $3d_{3/2}$ (blue) levels in CH_3I. The error bars represent the standard error of the β parameters extracted from the fit. The corresponding theoretical (CMS–Xα) photoelectron anisotropy parameters are plotted for the I $3d_{5/2}$ (magenta) and I $3d_{3/2}$ (cyan) levels using the experimental ionization energies.

electrons, approximating a single site emitter, allows a simple in-phase–out-of-phase interference pattern to emerge, resulting from on-axis back-scattering from the methyl group. This back-scattering is most pronounced for a_1 symmetry outgoing waves due to the axial electron continuum density between the carbon and iodine atoms.

4. I 3d shake-up/shake-off spectrum

Figure 9(a) shows the photoelectron spectrum of CH_3I, recorded at a photon energy of 740 eV, in the binding energy range encompassing the peaks associated with the I $3d_{5/2}^{-1}$ and I $3d_{3/2}^{-1}$ states, and the structure due to shake-up/shake-off satellites. Most of the distinct satellite structure is associated with the $3d_{3/2}^{-1}$ state, as the analogous features associated with the $3d_{5/2}^{-1}$ state are hidden by the main-line corresponding to the $3d_{3/2}^{-1}$ state.

We start our interpretation of the satellite structure by considering peaks which can be assigned to shake-up processes accompanying $3d_{3/2}$ ionization. Features observed at binding energies of 642.8 and 644.5 eV [labeled 3 and 4 in Fig. 9(b)], corresponding to energies of 4.5 and 6.2 eV above the main-line at 638.2 eV, are tentatively assigned to $3d_{3/2}$ ionization accompanied by the $2e \rightarrow \sigma^*$ and $2e \rightarrow 6s$ excitations, respectively. In the valence shell absorption spectrum of CH_3I, the bands due to the $2e \rightarrow \sigma^*$ and $2e \rightarrow 6s$ transitions are observed at ~4.8 and 6.2 eV,[63,64] respectively.

At higher energies, peaks observed at 647.9, 650.8, and 653.0 eV [labeled 5–7 in Fig. 9(b)], corresponding to energies of 9.6, 12.5, and 14.7 eV above the main-line, are tentatively assigned to $3d_{3/2}$ ionization accompanied by excitation of another electron from the 2e, $3a_1$, or 1e orbitals, respectively, into a Rydberg orbital. Vertical ionization energies of ~9.5, 12.5, and 14.7 eV have been reported[48] for the $\tilde{X}\,^2E_{3/2}$, $\tilde{A}\,^2A_1$, and $\tilde{B}\,^2E$ states, respectively.

Two features, labeled 1 and 2 in Fig. 9(b), are analogous to peaks 3 and 4 but involve $3d_{5/2}$ ionization. Peak 1 at 633.0 eV, and the shoulder (peak 2) at 636.5 eV, can be assigned to shake-up satellites, where $3d_{5/2}$ ionization is accompanied by the excitation of an electron from the outermost 2e orbital into the 6s Rydberg orbital, and by excitation from the 2e orbital into a high lying Rydberg orbital connected with the $\tilde{X}\,^2E_{3/2}$ limit, respectively.

In addition to these shake-up satellites, a continuum associated with shake-off transitions starts at a binding energy of ~634 eV and extends to at least 670 eV.

Figure 9(c) shows that the β parameters associated with the satellite structure are similar to those of the main-lines.

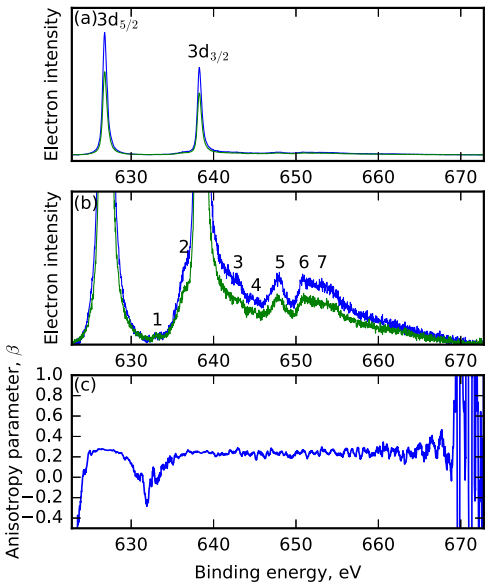

FIG. 9. Photoelectron spectra of CH_3I, recorded at a photon energy of 740 eV, using parallel (blue) and perpendicular (green) linearly polarized radiation, in the binding energy range encompassing structure due to the I $3d_{5/2,3/2}$ main-lines and the associated shake-up/shake-off satellites. Panel (a) shows the entire spectrum. Panel (b) shows an expanded view, highlighting the structure due to the shake-up/shake-off satellites. Possible assignments for the numbered peaks are given in the text. Panel (c) shows the photoelectron anisotropy parameter, where a 10-point moving average has been applied to improve the signal-to-noise ratio. The dip on the β values at binding energies around 632 eV is an experimental artefact caused by the low electron intensity.

5. Measurements of the $M_5N_{45}N_{45}$ and $M_4N_{45}N_{45}$ Auger electron yields

A simple, indirect method of determining the relative photoionization cross sections of the I $3d_{5/2}$ and I $3d_{3/2}$ orbitals in CH_3I is through a measurement of the $M_5N_{45}N_{45}$ and $M_4N_{45}N_{45}$ Auger electron yields.[13] As, for example, the first step in the $M_5N_{45}N_{45}$ Auger decay is the formation of the I $3d_{5/2}^{-1}$ hole state, the $M_5N_{45}N_{45}$ Auger electron yield is directly proportional to the I $3d_{5/2}$ photoionization partial cross section. In our experiment, the $M_5N_{45}N_{45}$ and $M_4N_{45}N_{45}$ yields were determined by selecting an electron kinetic energy window, with a width of ~10 eV, centred at ~497 and 507 eV, respectively [Fig. 5(b)]. These windows omit the peak due to the transition into the $^1S_0$ final state[49] but ensure that all of the detected Auger electron signal is associated with the selected decay. The yields shown in Fig. 10 were recorded using perpendicular linearly polarized radiation. At photon energies close to the I $3d_{5/2}$ and $3d_{3/2}$ ionization thresholds at 626.8 and 638.3 eV, respectively, direct photoionization of the I 4p orbital can lead to a small contribution from

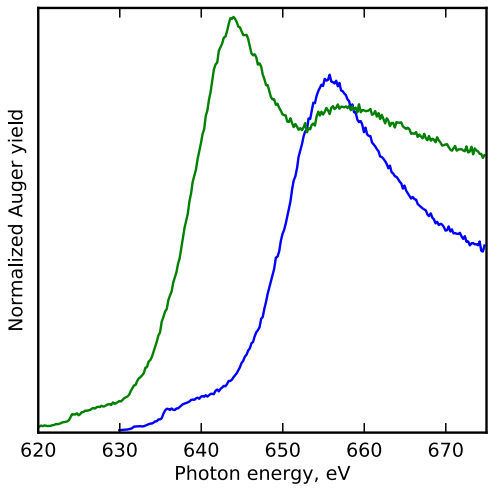

FIG. 10. The $M_4N_{45}N_{45}$ (blue) and $M_5N_{45}N_{45}$ (green) Auger electron yields of CH_3I recorded with perpendicular linearly polarized radiation.

electrons whose kinetic energies overlap with those of the Auger electrons due to the $M_{45}N_{45}N_{45}$ transitions. Hence, the Auger electron signal remains finite at threshold. This overlap in kinetic energies only occurs near threshold and does not affect the shape of the yields in the regions of interest containing the shape resonances.

Our $M_5N_{45}N_{45}$ Auger electron yield shows a peak at 644.0 eV, corresponding to the $3d_{5/2} \rightarrow \varepsilon f$ shape resonance, followed by a broad maximum centred at ~657.4 eV. In contrast, the $M_4N_{45}N_{45}$ yield displays a single peak at 655.7 eV associated with the $3d_{3/2} \rightarrow \varepsilon f$ shape resonance. The photon energies corresponding to the positions of the shape resonances in the Auger electron yields coincide well with those observed in the total ion yield. The overall shape of the Auger electron yields measured in the present experiment for the I 3d level in CH_3I is similar to that of the corresponding yields determined for the Xe 3d level[13] and that of the calculated Xe 3d photoionization partial cross sections.[1–3]

In xenon, the theoretical work showed that the second (higher energy) maximum in the Xe $3d_{5/2}$ photoionization partial cross section was the result of interchannel coupling between the $3d_{5/2}$ and $3d_{3/2}$ continua.[1–3] Specifically, the coupling mixes a small amount of the continuum wavefunctions representing the $3d_{3/2}$ channels with those representing the $3d_{5/2}$ channels.[1] However, this mixing does not occur only between states of the same energy. Thus, the second maximum in the calculated $3d_{5/2}$ cross section does not occur at exactly the same energy as the maximum in the $3d_{3/2}$ cross section.[1] In xenon, the second maximum is observed at an energy ~3 eV higher than that of the peak in the $3d_{3/2}$ cross section.[13]

Given the similarity between the Xe $M_{45}N_{45}N_{45}$ Auger electron yields[13] and those for the I $M_{45}N_{45}N_{45}$ transition measured in the present experiment, it appears reasonable to suggest that interchannel coupling between the I $3d_{5/2}$ and I $3d_{3/2}$ continua is responsible for the maximum observed at 657.4 eV in the $M_5N_{45}N_{45}$ yield. In CH_3I, the second maximum in the $M_5N_{45}N_{45}$ yield is shifted to higher energy by ~1.7 eV compared to the position of the peak in the $M_4N_{45}N_{45}$ yield.

VI. SUMMARY

The total ion yield of CH_3I has been measured using synchrotron radiation in the vicinity of the I $3d_{5/2,3/2}$ thresholds and exhibits broad maxima associated with the $3d \rightarrow \varepsilon f$ shape resonances. The corresponding theoretical absorption cross section indicates that, above the ionization threshold, transitions into the f($l = 3$) continuum channel dominate.

The complete photoelectron spectrum of CH_3I has been recorded at several photon energies, and bands due to the C 1s, I 3d, 4s, 4p, and 4d atomic-like orbitals, as well as the molecular valence orbitals, have been observed and assigned. The photoelectron band associated with the I 4p orbital has an unusual appearance due to the rapid decay of the $4p^{-1}$ hole state through Coster-Kronig and super-Coster-Kronig transitions.

The experimentally derived β parameters for the I 3d orbital have been compared to the corresponding theoretical results, calculated using the CMS–Xα approach, and a satisfactory agreement has been found. The I 3d shake-up/shake-off spectrum has been recorded, and some of the satellite structure has been assigned. The β parameters associated with the shake-up/shake-off satellites are similar to those characterizing the main-lines.

The $M_5N_{45}N_{45}$ and $M_4N_{45}N_{45}$ Auger electron yields have been measured in the photon energy range encompassing the $3d \rightarrow \varepsilon f$ shape resonances. Each yield curve exhibits a maximum associated with the corresponding continuum resonance, but that for the $M_5N_{45}N_{45}$ decay contains an additional maximum due to interchannel coupling between the $3d_{5/2}$ and $3d_{3/2}$ continua.

SUPPLEMENTARY MATERIAL

See supplementary material for descriptions of the ion spectrometer and the photoelectron peak fitting procedure and for a discussion of the I $3d_{5/2}$:$3d_{3/2}$ branching ratio.

ACKNOWLEDGMENTS

R.F. is grateful to the Engineering and Physical Sciences Research Council (EPSRC) for a research studentship. D.R. acknowledges support by the Chemical Sciences, Geosciences, and Biosciences Division, Office of Basic Energy Sciences, Office of Science, U.S. Department of Energy under Award No. DE-FG02-86ER13491. S.T.P. was supported by the U. S. Department of Energy, Office of Science, Office of Basic Energy Sciences, Division of Chemical Sciences, Geosciences, and Biosciences under Contract No. DE-AC02-06CH11357. N.A.B. is grateful for support from the EPSRC [Grant No. EP/N002148/1]. D.M.P.H. is grateful to the Science and Technology Facilities Council (United Kingdom) for financial support. We are grateful to the SOLEIL staff for running the facility and providing beamtime under Project No. 20150786.

[1] M. Ya. Amusia, L. V. Chernysheva, S. T. Manson, A. M. Msezane, and V. Radojević, Phys. Rev. Lett. **88**, 093002 (2002).
[2] D. Toffoli, M. Stener, and P. Decleva, J. Phys. B: At. Mol. Opt. Phys. **35**, 1275 (2002).
[3] V. Radojević, D. M. Davidović, and M. Ya. Amusia, Phys. Rev. A **67**, 022719 (2003).
[4] R. D. Deslattes, Phys. Rev. Lett. **20**, 483 (1968).
[5] O. Yağci and J. E. Wilson, J. Phys. C: Solid State Phys. **16**, 383 (1983).
[6] U. Gelius, J. Electron Spectrosc. Relat. Phenom. **5**, 985 (1974).
[7] S. Svensson, B. Eriksson, N. Mårtensson, G. Wendin, and U. Gelius, J. Electron Spectrosc. Relat. Phenom. **47**, 327 (1988).
[8] B. Sonntag, T. Nagata, Y. Sato, Y. Satow, A. Yagishita, and M. Yanagihara, J. Phys. B: At. Mol. Phys. **17**, L55 (1984).
[9] M. Kato, Y. Morishita, M. Oura, H. Yamaoka, Y. Tamenori, K. Okada, T. Matsudo, T. Gejo, I. H. Suzuki, and N. Saito, J. Electron Spectrosc. Relat. Phenom. **160**, 39 (2007).
[10] N. Saito and I. H. Suzuki, J. Phys. B: At. Mol. Phys. **25**, 1785 (1992).
[11] U. Arp, K. Iemura, G. Kutluk, T. Nagata, S. Yagi, and A. Yagishita, J. Phys. B: At. Mol. Phys. **32**, 1295 (1999).
[12] S. H. Southworth, R. Wehlitz, A. Pićon, C. S. Lehmann, L. Cheng, and J. F. Stanton, J. Chem. Phys. **142**, 224302 (2015).
[13] A. Kivimäki, U. Hergenhahn, B. Kempgens, R. Hentges, M. N. Piancastelli, K. Maier, A. Rüdel, J. J. Tulkki, and A. M. Bradshaw, Phys. Rev. A **63**, 012716 (2000).
[14] D. J. Kennedy and S. T. Manson, Phys. Rev. A **5**, 227 (1972).
[15] M. Ya. Amusia and V. K. Ivanov, Phys. Lett. A **65**, 217 (1978).
[16] M. Kutzner, V. Radojević, and H. P. Kelly, Phys. Rev. A **40**, 5052 (1989).
[17] S. Hirata and M. Head-Gordon, Chem. Phys. Lett. **314**, 291 (1999).

[18]D. Dill and J. L. Dehmer, J. Chem. Phys. **61**, 692 (1974).
[19]J. W. Davenport, Ph.D. dissertation (University of Pennsylvania, 1976).
[20]B. Erk *et al.*, Science **345**, 288 (2014).
[21]K. Schnorr *et al.*, Phys. Rev. Lett. **113**, 073001 (2014).
[22]R. Boll *et al.*, Struct. Dyn. **3**, 043207 (2016).
[23]F. Brausse, G. Goldsztejn, K. Amini, R. Boll, S. Bari, C. Bomme, M. Brouard, M. Burt, B. Cunha de Miranda, S. Düsterer, B. Erk, M. Géléoc, R. Geneaux, A. S. Gentleman, R. Guillemin, I. Ismail, P. Johnsson, L. Journel, T. Kierspel, H. Köckert, J. Küpper, P. Lablanquie, J. Lahl, J. W. L. Lee, S. R. Mackenzie, S. Maclot, B. Manschwetus, A. S. Mereshchenko, T. Mullins, P. K. Olshin, J. Palaudoux, S. Patchkovskii, F. Penent, M. N. Piancastelli, D. Rompotis, T. Ruchon, A. Rudenko, E. Savelyev, N. Schirmel, S. Techert, O. Travnikova, S. Trippel, J. G. Underwood, C. Vallance, J. Wiese, M. Simon, D. M. P. Holland, T. Marchenko, A. Rouzée, and D. Rolles, Phys. Rev. A **97**, 043429 (2018).
[24]A. Stolow and J. G. Underwood, Adv. Chem. Phys. **139**, 497 (2008).
[25]J. Söderström, A. Lindblad, A. N. Grum-Grzhimailo, O. Travnikova, C. Nicolas, S. Svensson, and C. Miron, New J. Phys. **13**, 073014 (2011).
[26]I. Powis, D. M. P. Holland, E. Antonsson, M. Patanen, C. Nicolas, C. Miron, M. Schneider, D. Yu. Soshnikov, A. Dreuw, and A. B. Trofimov, J. Chem. Phys. **143**, 144304 (2015).
[27]H. Petersen, Opt. Commun. **40**, 402 (1982).
[28]N. Kosugi, E. Shigemasa, and A. Yagishita, Chem. Phys. Lett. **190**, 481 (1992).
[29]P. Baltzer, L. Karlsson, M. Lundqvist, and B. Wannberg, Rev. Sci. Instrum. **64**, 2179 (1993).
[30]J. Cooper and R. N. Zare, J. Chem. Phys. **48**, 942 (1968).
[31]S. Svensson, N. Mårtensson, E. Basilier, P. Å. Malmquist, U. Gelius, and K. Siegbahn, Phys. Scr. **14**, 141 (1976).
[32]L. O. Werme, T. Bergmark, and K. Siegbahn, Phys. Scr. **6**, 141 (1972).
[33]J. Jauhiainen, A. Ausmees, A. Kivimäki, S. J. Osborne, A. Naves de Brito, S. Aksela, S. Svensson, and H. Aksela, J. Electron Spectrosc. Relat. Phenom. **69**, 181 (1994).
[34]A. Niehaus, J. Phys. B: At. Mol. Phys. **10**, 1845 (1977).
[35]V. Schmidt, *Electron Spectrometry of Atoms using Synchrotron Radiation* (Cambridge University Press, Cambridge, 1997).
[36]G. B. Armen, J. Tulkki, T. Åberg, and B. Crasemann, Phys. Rev. A **36**, 5606 (1987).
[37]M. Stener, G. Fronzoni, and M. de Simone, Chem. Phys. Lett. **373**, 115 (2003).
[38]T. Yanai, D. P. Tew, and N. C. Handy, Chem. Phys. Lett. **393**, 51 (2004).
[39]L. S. C. Martins, F. A. L. de Souza, G. A. Ceolin, F. E. Jorge, R. C. de Berredo, and C. T. Campos, Comput. Theor. Chem. **1013**, 62 (2013).
[40]N. A. Besley, A. T. B. Gilbert, and P. M. W. Gill, J. Chem. Phys. **130**, 124308 (2009).
[41]M. Stener, P. Decleva, and A. Lisini, J. Electron Spectrosc. Relat. Phenom. **74**, 29 (1995).
[42]I. Powis, Chem. Phys. **201**, 189 (1995).
[43]D. M. P. Holland, I. Powis, G. Öhrwall, L. Karlsson, and W. von Niessen, Chem. Phys. **326**, 535 (2006).
[44]A. P. Hitchcock and C. E. Brion, J. Electron Spectrosc. Relat. Phenom. **13**, 193 (1978).
[45]N. A. Besley and F. A. Asmuruf, Phys. Chem. Chem. Phys. **12**, 12024 (2010).
[46]D. W. Lindle, P. H. Kobrin, C. M. Truesdale, T. A. Ferrett, P. A. Heimann, H. G. Kerkhoff, U. Becker, and D. A. Shirley, Phys. Rev. A **30**, 239 (1984).
[47]G. O'Sullivan, J. Phys. B: At. Mol. Phys. **15**, L327 (1982).
[48]L. Karlsson, R. Jadrny, L. Mattsson, F. T. Chau, and K. Siegbahn, Phys. Scr. **16**, 225 (1977).
[49]R. Forbes, A. De Fanis, C. Bomme, D. Rolles, S. T. Pratt, I. Powis, N. A. Besley, S. Nandi, A. R. Milosavljević, C. Nicolas, J. D. Bozek, J. G. Underwood, and D. M. P. Holland, J. Chem. Phys. **149**, 094304 (2018).
[50]A. P. Lukirskii, T. M. Zimkina, and I. A. Britov, Izv. Akad. Nauk. SSSR, Ser. Fiz. **28**, 772 (1964).
[51]K. Codling and R. P. Madden, Appl. Opt. **4**, 1431 (1965).
[52]L. S. Cederbaum, W. Domcke, J. Schirmer, and W. von Niessen, Adv. Chem. Phys. **65**, 115 (1986).
[53]W. Mehlhorn, in *Atomic Inner-Shell Physics*, edited by B. Crasemann (Plenum Press, New York, 1985), p. 119.
[54]D. Coster and R. Kronig, Physica **2**, 13 (1935).
[55]E. J. McGuire, Phys. Rev. A **5**, 1043 (1972).
[56]G. Wendin and M. Ohno, Phys. Scr. **14**, 148 (1976).
[57]G. Wendin and M. Ohno, in *Proceeding of the 2nd International Conference on Inner Shell Ionization Phenom*, edited by W. Mehlhorn (Freiburg, 1976), p. 166.
[58]H. Siegbahn and L. Karlsson, in *Handbuch der Physik*, edited by W. Mehlhorn (Springer-Verlag, Berlin, 1982), Vol. 31, p. 215.
[59]V. Schmidt, Rep. Prog. Phys. **55**, 1483 (1992).
[60]U. Becker, D. Szostak, H. G. Kerkhoff, M. Kupsch, B. Langer, R. Wehlitz, A. Yagishita, and T. Hayaishi, Phys. Rev. A **39**, 3902 (1989).
[61]T. X. Carroll, R. W. Shaw, T. D. Thomas, C. Kindle, and N. Bartlett, J. Am. Chem. Soc. **96**, 1989 (1974).
[62]M. Jurvansuu, A. Kivimäki, and S. Aksela, Phys. Rev. A **64**, 012502 (2001).
[63]A. Fahr, A. K. Nayak, and M. J. Kurylo, Chem. Phys. **197**, 195 (1995).
[64]R. Locht, B. Leyh, H. W. Jochims, and H. Baumgärtel, Chem. Phys. **365**, 109 (2009).